THIS MANUSCRIPT HAS BEEN SUBMITTED TO THE JOURNAL OF GLACIOLOGY AND HAS NOT BEEN PEER-REVIEWED.

Modification of Antarctic geothermal heat flux by groundwater flow

Journal:	*Journal of Glaciology*
Manuscript ID	Draft
Manuscript Type:	Article
Date Submitted by the Author:	n/a
Complete List of Authors:	Cairns, Gabriel; University of Oxford, Mathematical Institute Benham, Graham; University College London, Department of Mechanical Engineering Hewitt, Ian; University of Oxford, Mathematical Institute
Keywords:	Subglacial sediments, Subglacial processes, Melt - basal, Ice-sheet modelling
Abstract:	The geothermal heat flux to the bed of the ice in Antarctica is important for ice flow and basal meltwater production, but is also highly uncertain. In particular, it is thought that groundwater flow in sedimentary basins could modify the geothermal heat flux to the ice bed by advecting heat, but this process is unaccounted for in current models. In this paper, we develop a mathematical model to investigate the effect of three-dimensional groundwater flow, driven by topography and sediment compaction, on subglacial heat transport. We then obtain a reduced-order approximate solution to this model. Using this approximate solution combined with geophysical data, we find that groundwater flow could enhance or reduce geothermal heat flux by tens of mW/m2 across large regions of Antarctica. We find that topographically-driven groundwater flow enhances heat flux in the centre of ice streams and reduces it at the margins, while compaction-driven groundwater flow enhances heat flux beneath thinning ice and reduces it beneath thickening ice. Our results provide insight into the possible effect of groundwater flow on Antarctic

	geothermal heat flux, and highlight the need for further investigation into the properties of Antarctic sedimentary basins.

Modification of Antarctic geothermal heat flux by groundwater flow

Gabriel CAIRNS[1], Graham BENHAM[2], Ian HEWITT[1]

[1] *Mathematical Institute, University of Oxford, Oxford, UK*

[2] *Department of Mechanical Engineering, University College London, London, UK*

Correspondence: Gabriel Cairns <gabriel.cairns@maths.ox.ac.uk>

ABSTRACT. The geothermal heat flux to the bed of the ice in Antarctica is important for ice flow and basal meltwater production, but is also highly uncertain. In particular, it is thought that groundwater flow in sedimentary basins could modify the geothermal heat flux to the ice bed by advecting heat, but this process is unaccounted for in current models. In this paper, we develop a mathematical model to investigate the effect of three-dimensional groundwater flow, driven by topography and sediment compaction, on subglacial heat transport. We then obtain a reduced-order approximate solution to this model. Using this approximate solution combined with geophysical data, we find that groundwater flow could enhance or reduce geothermal heat flux by tens of mW m^{-2} across large regions of Antarctica. We find that topographically-driven groundwater flow enhances heat flux in the centre of ice streams and reduces it at the margins, while compaction-driven groundwater flow enhances heat flux beneath thinning ice and reduces it beneath thickening ice. Our results provide insight into the possible effect of groundwater flow on Antarctic geothermal heat flux, and highlight the need for further investigation into the properties of Antarctic sedimentary basins.

For Peer Review

1. INTRODUCTION

The Antarctic ice sheet is the largest body of ice on the planet, with the potential to contribute an estimated 30 cm of sea-level rise by 2100 and up to 6.9 m by 2300 under high-emission climate scenarios (Seroussi and others, 2024). One of the largest sources of uncertainty in predicting future Antarctic ice loss is the thermal state of the ice bed, with a warmer ice bed leading to higher predicted ice loss (Dawson and others, 2022). In particular, the geothermal heat flux, which heats the ice bed alongside frictional heating, is relatively ill-constrained, with significant variation between models (Reading and others, 2022). This heat flux consists of conduction from the mantle, alongside radiogenic heat production in the crust (Stål and others, 2021).

Geothermal heat flux influences ice flow via the temperature-dependent rheology of the ice. It also facilitates sliding of the ice by thawing the bed, and by contributing to the production of meltwater, which enters the subglacial hydrological system (Burton-Johnson and others, 2020). As a result, localised regions of elevated geothermal heat flux can significantly influence ice dynamics (Pittard and others, 2016). Moreover, resolving small-scale variations in geothermal heat flux can lead to higher overall estimated melt rates (McCormack and others, 2022).

One source of uncertainty in current models of Antarctic geothermal heat flux is the role of groundwater, significant volumes of which are stored in sedimentary basins (Gustafson and others, 2022; Aitken and others, 2023). These sedimentary basins underlie large portions of Antarctica, including many of its fastest-flowing ice streams (Li and others, 2022; Li and Aitken, 2024). It is believed that the circulation of this groundwater could, by advecting heat, produce local variations in geothermal heat flux (Gooch and others, 2016; Tankersley and others, 2022; Reading and others, 2022). However, existing models of Antarctic geothermal heat flux (*e.g.* Stål and others, 2021) do not account for possible effects of groundwater, owing in part to the large uncertainty regarding the hydraulic properties of sedimentary basins.

Conversely, while there have been several attempts to model large-scale groundwater flow in sedimentary basins (*e.g.* Li and others, 2022; Robel and others, 2023; Cairns and others, 2025), so far these have not considered the effect of groundwater flow on heat transport. In a notable exception, Gooch and others (2016) found, using a one-dimensional vertical model, that groundwater flow upwards and downwards could significantly enhance or reduce geothermal heat flux. In addition, Christoffersen and Tulaczyk (2003) considered groundwater flow and energy transport in a one-dimensional mathematical model for freezing

For Peer Review

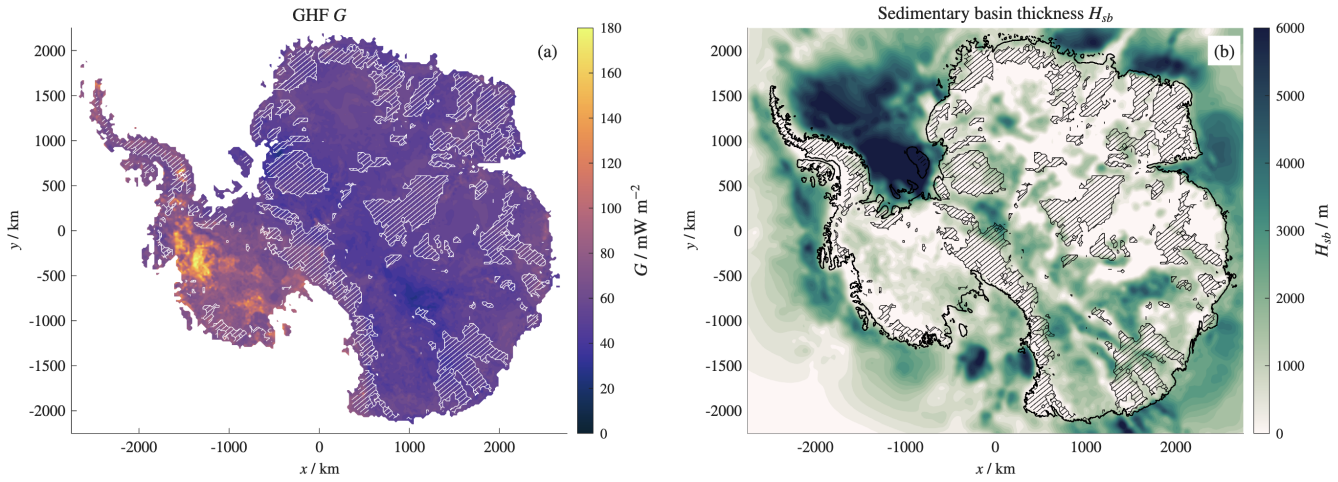

Fig. 1. (a) Modelled Antarctic geothermal heat flux (without modification by groundwater flow) from Stål and others (2021). (b) Modelled sedimentary basin thickness from Li and Aitken (2024). Probable frozen regions of the ice bed, based on Seiner and others (2025), are masked with hatches in both instances.

and thawing near the ice bed. However, these models do not include horizontal groundwater flow, which is important for variations across Antarctica.

In this paper, we present a mathematical model for groundwater flow in a sedimentary basin, including both horizontal and vertical flow and sediment compaction, combined with heat transport. We explore the predictions of this model in an idealised cross-section of an Antarctic sedimentary basin, and derive a reduced-order approximation for the modification of the geothermal heat flux by groundwater flow. We then apply this approximation to existing geophysical models of Antarctic heat flux and sedimentary basin thickness, in order to investigate the extent to which groundwater flow could modify the heat flux. We find that, for realistic parameter values, groundwater flow has the potential to significantly enhance or reduce heat flux in large regions of both East and West Antarctica, with the resulting difference in basal melting comparable in size to the exfiltration of water from the sedimentary basin. In particular, topographically-driven groundwater flow enhances heat flux in the centre of ice streams and reduces it at the margins, potentially helping the ice stream to self-reinforce. Meanwhile, compaction-driven groundwater flow provides a positive feedback by enhancing heat flux beneath thinning ice and reducing it beneath thickening ice.

In Section 2 we describe the governing equations of the model, in dimensional and dimensionless form, and in Section 3 we provide an example solution for a synthetic geometry in two dimensions. In Section 4 we then derive an approximate solution for the modification of the geothermal heat flux, and compare this approximate solution with the numerical solution for the aforementioned example. We then evaluate

For Peer Review

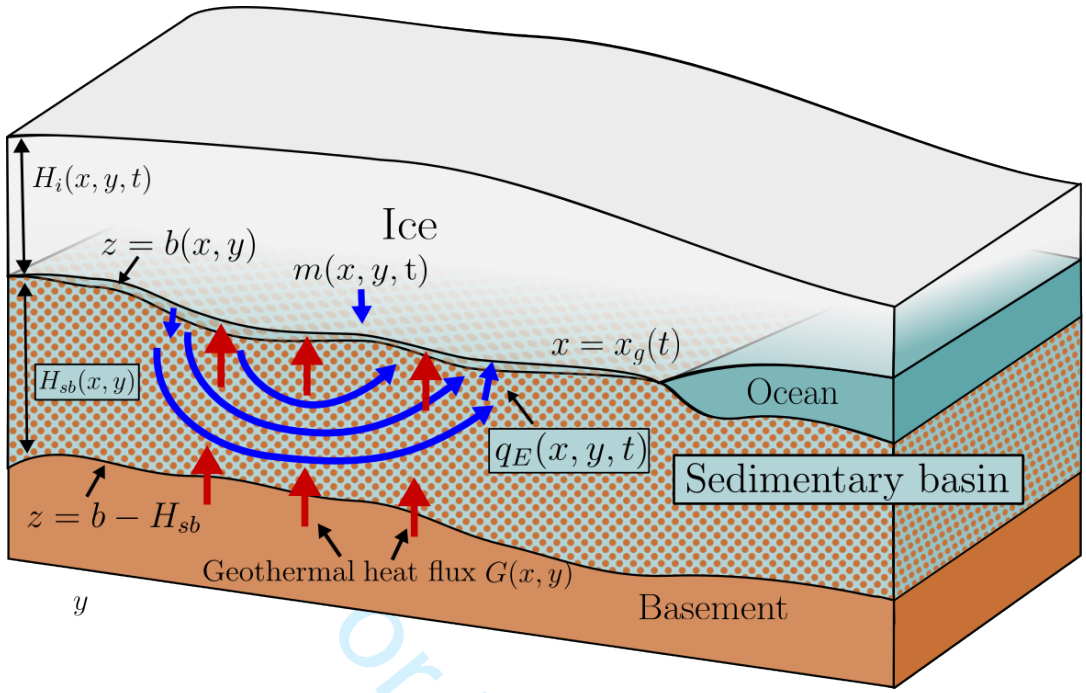

Fig. 2. Schematic of the model. The ice sheet has thickness H_i and bed at $z = b$. It overlies a sedimentary basin with thickness H_{sb} and an impermeable lower boundary. There is a geothermal heat flux G into the sedimentary basin, which is modified by groundwater flow on its way to the ice bed.

this approximate modified heat flux for Antarctic data in Section 5, and discuss our findings.

2. MODEL

We consider energy transport and groundwater flow in a sedimentary basin with thickness $H_{sb}(x, y)$, whose upper surface lies at the ice-bed interface $z = b(x, y)$. The bottom of the sedimentary basin is at $z = b-H_{sb}$. Above the sedimentary basin is an ice sheet with thickness $H_i(x, t)$, and between the sedimentary basin and the ice is a subglacial hydrological system, which we model as a thin layer of pressurised water. We use subscripts sb, i, h, w and r for properties of the sedimentary basin, ice, hydrological system, water and sedimentary rock. We consider longer timescales (*i.e.* hundreds to thousands of years), so that annual variability is not important. In particular, we will generally assume that groundwater and heat dynamics are in a quasi-steady state.

We also make the assumption that the vertical aspect ratio is small, *i.e.* the vertical lengthscale of the sedimentary basin is much smaller than the horizontal lengthscale. This is consistent with geophysical estimates of Antarctic geology, where sedimentary basins are usually a few kilometers thick and hundreds to thousands of kilometers wide (Tankersley and others, 2022; Li and Aitken, 2024). This is a frequent

For Peer Review

assumption in models of groundwater flow, where it is referred to as the Dupuit approximation. A further consequence of this approximation is that horizontal diffusion of heat is negligible compared to vertical diffusion, but we note that vertical and horizontal advection are generally comparable. Our model therefore improves on existing one-dimensional models, which do not include horizontal advection.

2.1 Governing equations

The temperature in the sedimentary basin $T_{sb}(x, y, z, t)$ is governed by an advection-diffusion equation,

$$\rho_{sb} C_{sb} \frac{\partial T_{sb}}{\partial t} + \rho_w C_w \mathbf{u_{sb}} \cdot \nabla T_{sb} + \rho_w C_w w_{sb} \frac{\partial T_{sb}}{\partial z} = k_{sb} \frac{\partial^2 T}{\partial z^2} + Q_r + D_{sb}. \tag{1}$$

Here $\mathbf{u_{sb}}(x, y, z, t)$ and $w_{sb}(x, y, z, t)$ are the horizontal and vertical components of the Darcy flux in the sedimentary basin, and $\nabla = (\partial/\partial x, \partial/\partial y)$ is the horizontal components of the gradient. We include a source term Q_r for radiogenic heating, and D_{sb} for dissipation in the groundwater flow. We neglect thermal dispersion, which we expect to be negligible compared to diffusion (Bear, 2013).

We use ρ, C and k to refer to density, specific heat and thermal conductivity, all assumed constant for simplicity. The bulk quantities $\rho_{sb} C_{sb}$ and k_{sb} are defined in terms of the porosity ϕ as

$$\rho_{sb} C_{sb} = \rho_r C_r (1 - \phi) + \rho_w C_w \phi, \quad k_{sb} = k_r (1 - \phi) + k_w \phi. \tag{2}$$

Note that advection only occurs in the water phase.

For simplicity, we make the assumption of a temperate (thawed) bed, and ignore the dependence of the melting temperature on pressure. Although large regions of Antarctica likely possess a frozen bed, the assumption of a thawed bed is reasonable beneath most outlet glaciers where ice dynamics are of most concern. We therefore impose that the top of the sedimentary basin is at a uniform melting temperature T_m.

$$T_{sb} = T_m \quad \text{on} \quad z = b. \tag{3}$$

At the bottom, we prescribe a conductive heat flux given by the geothermal heat $G(x, y)$,

$$-k_{sb} \frac{\partial T_{sb}}{\partial z} = G \quad \text{on} \quad z = b - H_{sb}. \tag{4}$$

In order to determine the Darcy flux components $\mathbf{u_{sb}}$ and w_{sb}, we treat the sedimentary basin as a

For Peer Review

weakly compressible porous medium under uniaxial strain. This implies that the pressure p_{sb} obeys the groundwater flow equation (Robel and others, 2023)

$$S_s \frac{\partial p_{sb}}{\partial t} + \rho_w g \left(\nabla \cdot \mathbf{u_{sb}} + \frac{\partial w_{sb}}{\partial z} \right) = S_s \xi \frac{\partial p_h}{\partial t}, \tag{5}$$

where p_h is the water pressure in the hydrological system, and the constants S_s and $0 < \xi < 1$ are the specific storage and Skempton's coefficient respectively. These terms allow for compaction of the porous medium, which produces a vertical flow in response to changes in the total loading stress. If we set $S_s(1-\xi)$ to 0, we recover the limit of incompressible groundwater flow. The water pressure is given by the overburden pressure due to the weight of the ice sheet, minus the so-called effective pressure N, which encapsulates the resistance of the subglacial hydrological system to compression,

$$p_h = \rho_i g H_i - N. \tag{6}$$

We also employ the aforementioned Dupuit approximation, which implies that the pressure p_{sb} is approximately hydrostatic,

$$p_{sb} \approx p_h + \rho_w g (b - z). \tag{7}$$

Assuming that the Darcy flux components are given by Darcy's law, we have that

$$\mathbf{u_{sb}} = -\rho_w g K_{sb} \nabla p_{sb} = -K_{sb} \nabla \psi, \tag{8}$$

where K_{sb} is the hydraulic conductivity and

$$\psi = \frac{p_h}{\rho_w g} + b = \frac{1}{\rho_w g} \left(\rho_i g H_i - N \right) + b, \tag{9}$$

is the hydraulic head. The hydraulic conductivity is given by

$$K_{sb} = \rho_w g k^p_{sb} / \mu, \tag{10}$$

where k^p_{sb} denotes the permeability of the porous medium, and μ is the viscosity of water. Throughout this paper we work in terms of K_{sb} rather than k^p_{sb}, in order to avoid confusion with the thermal conductivity.

Both K_{sb} and S_s are properties of the porous medium that are not well constrained, the former because

For Peer Review

of its dependence on k^p_{sb}, which is an unknown property of the rock matrix. Therefore, a range of values for each should be considered. For example, Robel and others (2023) consider permeabilities that give K_{sb} ranging from 10^{-10} to 10^{-6} ms^{-1} and S_S from 10^{-7} to 10^{-4} m^{-1}.

Assuming that there is no normal flux through the bottom of the sedimentary basin,

$$w_{sb} = \mathbf{u_{sb}} \cdot \nabla(b - H_{sb}) \quad \text{on} \quad z = b - H_{sb}, \tag{11}$$

we may obtain the vertical Darcy flux by integrating Equation (5), using Equations (7) and (8) for p and $\mathbf{u_{sb}}$ respectively. This gives

$$w_{sb} = (z - b + H_{sb})\left(K_{sb}\nabla^2\psi - S_s(1-\xi)\frac{\partial\psi}{\partial t}\right) - K_{sb}\nabla(b - H_{sb}) \cdot \nabla\psi. \tag{12}$$

We define the exfiltration q_E (or infiltration if $q_E < 0$) to be the normal flux through the top of the sedimentary basin,

$$q_E = (w_{sb} - \mathbf{u_{sb}} \cdot \nabla b)|_{z=b} = \nabla \cdot (K_{sb}H_{sb}\nabla\psi) - S_s(1-\xi)H_{sb}\frac{\partial\psi}{\partial t}. \tag{13}$$

Finally, the dissipative heating term in the energy balance is given by

$$D_{sb} = K_{sb}\rho_w g|\nabla\psi|^2, \tag{14}$$

assuming that the horizontal fluxes are much larger than the vertical flux under the Dupuit approximation.

Under our assumption that the bed is at a uniform melting temperature T_m, the energy balance at the ice bed $z = b$ reads

$$\rho_w mL = -k_{sb}\frac{\partial T_{sb}}{\partial z} + k_i\frac{\partial T_i}{\partial z} + \tau_{\mathbf{b}} \cdot \mathbf{u_b} + D_h, \tag{15}$$

where the terms are as follows:

$\rho_w mL$ is the energy used to melt or freeze the ice, with m the melt rate and L the latent heat,

$-k_{sb}\partial T_{sb}/\partial z$ is conductive heat flux upwards from the sedimentary basin,

$k_i\partial T_i/\partial z$ is the conductive heat flux into the ice,

$\tau_{\mathbf{b}} \cdot \mathbf{u_b}$ is the frictional heating from the sliding of the ice (and resulting deformation of the till, etc.),

For Peer Review

where τ_b and $\mathbf{u_b}$ are the basal shear stress and ice velocity,

D_h is the heat produced by dissipation from the flow in the hydrological system.

Conduction into the ice is a sink, whereas the other terms are heat sources. The conductive heat flux from the sedimentary basin (the first term on the right) is our primary interest here. In the absence of groundwater flow, this is equal geothermal heat flux along with a possible radiative heating contribution

$$-k_{sb}\frac{\partial T_{sb}}{\partial z} = G + Q_r H_{sb}. \tag{16}$$

We anticipate that groundwater flow modifies this term, and will focus in the change in the basal melt rate m that results from this. The other terms in Equation (15) will be considered fixed, although we note that there could be additional feedbacks; for example, modified sliding rates could change the frictional heating term.

In solving this model, the ice thickness H_i is either provided by data or must be prescribed using an ice sheet model. In the 2D example solutions for a synthetic geometry that follow, we use a shallow-shelf ice sheet model with a Weertman sliding law, which is described in more detail in Appendix A. Equation (9) also requires us to prescribe the effective pressure N. A simple parameterisation is to take the effective pressure as a fixed fraction of the overburden (*e.g.* Gregov and others, 2023),

$$N = \nu \rho_i g H_i, \tag{17}$$

where we take $\nu = 0.1$ throughout this paper. A more detailed model of the effective pressure could be obtained by extending the model in this paper to include subglacial hydrology, a feature which we have largely omitted for simplicity. Models of subglacial hydrology typically relate N to the distribution of water in the hydrological system, which is in turn found by solving a water mass conservation equation in which m and q_E are source terms (*e.g.* Werder and others, 2013; Flowers, 2015; Sommers and others, 2018; Cairns and others, 2026).

For Peer Review

Table 1. Physical parameters and scales used in the model. Estimates of ϕ, k_r and ξ are taken from Gooch and others (2016), ρ_r from Li and others (2022) (supplementary information) and C_r from Bear (2013). The range of values of S_S are based on a typical value from Robel and others (2023), although we note values outside of the range considered are also physically plausible. The values of K_{sb} are inferred from k^p_{sb}, which in turn are based on Gooch and others (2016) and Cairns and others (2025). While lower values of K_{sb} are possible, we do not consider these here as the resulting values of Pe are so small as to be indistinguishable from zero. The scale $[G]$ is inferred from data (Stål and others, 2021), whereas the scales $[z]$, $[t]$, $[\Delta T]$ and $[m]$ are derived from other parameters and scales following the procedure detailed in Appendix B.

Parameter	Value	Units	Parameter	Value	Units
ρ_w	1000	kg m^{-3}	ξ	0.2	
ρ_r	2000	kg m^{-3}	K_{sb}	1×10^{-6}–5×10^{-6}	m s^{-1}
ρ_i	900	kg m^{-3}	k^p_{sb}	1×10^{-12}–5×10^{-12}	m^2
C_w	4200	J kg^{-1} K^{-1}	μ	1×10^{-3}	Pa s
C_r	700	J kg^{-1} K^{-1}	$[x]$	5×10^5	m
ϕ	0.3		$[z]$	871	m
k_r	2.8	W m^{-1} K^{-1}	$[t]$	2900	yr
k_w	0.56	W m^{-1} K^{-1}	$[G]$	60	mW m^{-2}
g	9.81	m s^{-2}	$[\Delta T]$	25	K
S_S	3×10^{-7}–3×10^{-6}	m^{-1}	$[m]$	5.7	mm yr^{-1}

Table 2. Derived dimensionless parameters used in the model.

Parameter	Value
κ	0.017—0.084
Σ	0.009—0.09
δ	0.1
λ_{sb}	340–1700
Pe	0.0052—0.026
Ξ_{sb}	0.083

For Peer Review

2.2 Non-dimensionalisation

We now non-dimensionalise the above model, in order to reduce the number of parameters and exploit the relative smallness of certain terms. That is, we write variables as

$$x = [x]\hat{x}, \quad z = [z]\hat{z}, \quad T - T_m = [\Delta T]\hat{T} \quad \ldots, \tag{18}$$

where square brackets [] denote constant scales and hats denote dimensionless variables. We then drop hats from variables for readability. We select the scales based on a combination of observation and balancing terms in the governing equations, as detailed in Appendix B.

Under our choice of scalings, the dimensionless exfiltration is given by

$$\hat{q}_E = \kappa\hat{\nabla}\cdot\left(\hat{H}_{sb}\hat{\nabla}\hat{\psi}\right) - \Sigma\hat{H}_{sb}\frac{\partial\hat{\psi}}{\partial\hat{t}}, \tag{19}$$

where

$$\kappa = \frac{[w_{sb}]}{[m]} = \frac{K_{sb}[z]^2\rho_w L}{[x]^2[G]}, \quad \Sigma = \frac{S_S(1-\xi)[z]^2\rho_w L}{[G][t]}. \tag{20}$$

The parameter κ determines the size of the topography-driven groundwater flow, and scales with the hydraulic conductivity K_{sb}. Likewise, the parameter Σ determines the size of the compaction-driven groundwater flow, and scales with the specific storage S_S. The dimensionless hydraulic head is

$$\hat{\psi} = (1-\delta)\hat{H}_i - \hat{N} + \hat{b}, \tag{21}$$

where

$$\delta = 1 - \rho_i/\rho_w, \tag{22}$$

and the dimensionless Darcy flux components are

$$\hat{\mathbf{u}}_{\mathbf{sb}} = -\hat{\nabla}\hat{\psi}, \quad \hat{w}_{sb} = \left(\hat{z} - \hat{b} + \hat{H}_{sb}\right)\left(\hat{\nabla}^2\hat{\psi} - \frac{\Sigma}{\kappa}\frac{\partial\hat{\psi}}{\partial\hat{t}}\right) - \hat{\nabla}\left(\hat{b} - \hat{H}_{sb}\right)\cdot\hat{\nabla}\hat{\psi}. \tag{23}$$

Equation (1) for the temperature in the sedimentary basin becomes

$$\lambda_{sb}\frac{\partial\hat{T}_{sb}}{\partial\hat{t}} + \hat{\mathbf{u}}_{\mathbf{sb}}\cdot\hat{\nabla}\hat{T}_{sb} + \hat{w}_{sb}\frac{\partial\hat{T}_{sb}}{\partial\hat{z}} = \frac{1}{\mathrm{Pe}}\left(\frac{\partial^2\hat{T}_{sb}}{\partial\hat{z}^2} + \hat{Q}_r\right) + \Xi_{sb}\left(\frac{\partial\hat{\psi}}{\partial\hat{x}}\right)^2, \tag{24}$$

For Peer Review

where

$$\lambda_{sb} = \frac{\rho_{sb} C_{sb} [x]^2}{\rho_w C_w K_{sb} [z][t]}, \quad \mathrm{Pe} = \frac{K_{sb} \rho_w C_w [z]^3}{k_{sb} [x]^2}, \quad \hat{Q}_r = \frac{Q_r [z]}{[G]}, \quad \Xi_{sb} = \frac{g k_{sb}}{C_w [G]}. \tag{25}$$

The parameter λ_{sb} represents the timescale of heat flow in the sedimentary basin relative to evolution of the ice sheet, $\hat{Q}_{sb}$ is the dimensionless radiative heating, and Ξ_{sb} represents the size of the dissipation. The parameter Pe is the Peclet number of the sedimentary basin, representing the importance of heat advection compared to diffusion. The boundary conditions are

$$\hat{T}_{sb} = 0 \quad \text{on} \quad \hat{z} = \hat{b}. \tag{26}$$

$$\frac{\partial \hat{T}_{sb}}{\partial \hat{z}} = -\hat{G} \quad \text{on} \quad \hat{z} = \hat{b} - \hat{H}_{sb}, \tag{27}$$

where

$$\hat{G} = G/[G]. \tag{28}$$

3. EXAMPLE SOLUTION FOR A SYNTHETIC GEOMETRY IN 2D

As an illustrative example, we consider a solution of this model in two dimensions (x, z), representing a cross-section of an ice stream along a flow-line, which is shown in Figure 3. The sedimentary basin thickness H_{sb} is given by a Gaussian function, whose thickening and shallowing in the direction of groundwater flow drives infiltration and exfiltration of groundwater. This shape is chosen purely in order to illustrate the typical influence of groundwater flow.

Figure 3(a) shows the streamlines of this groundwater flow, driven by the hydraulic gradient. This flow advects heat, causing the temperature to deviate from the unmodified solution $T_{sb} = G(b - z)/k_{sb}$. When heat is advected downwards, the thermal gradient $\partial T/\partial z$ at the top of the sedimentary basin becomes smaller. Conversely, when heat is advected upwards, the thermal gradient at the top of the sedimentary basin is larger.

This results in a modification of the heat flux to the ice bed, seen in Figure 3(b). The heat flux is lowered in regions of groundwater infiltration, but elevated in regions of exfiltration. A higher value of the hydraulic conductivity K_{sb}, hence the Péclet number Pe, amplifies this change, with the difference between the modified and unmodified flux approximately scaling with Pe.

In Figure 3(c), the effect of compaction-driven exfiltration is seen, for a spatially-uniform steady ice

For Peer Review

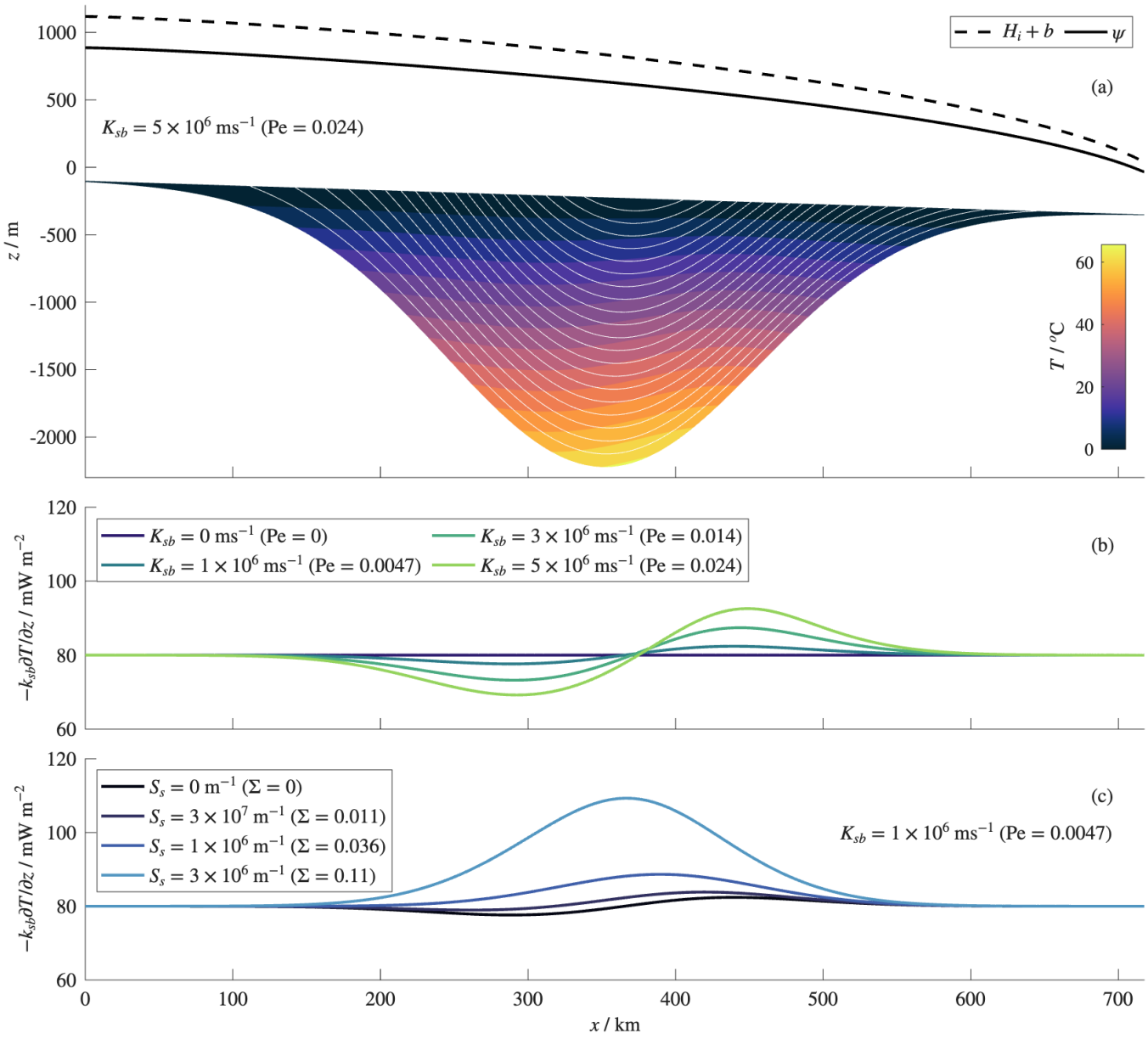

Fig. 3. Steady state solution for a test case with sedimentary basin thickness $H_{sb} = (2000\exp(-((x - 350\text{km})/150\text{km}))^2)$ m, and geothermal heat flux $G = 80\,\text{mW m}^{-2}$. (a) shows the ice profile and hydraulic potential ψ, along with the temperature in the sedimentary basin at 5° contours and streamlines of the groundwater flow for a relatively high hydraulic conductivity K_{sb} with $S_S = 0$. (b) and (c) show the modified heat flux to the ice bed for various values of K_{sb} with $S_S = 0$, and for various values of the specific storage S_S for a fixed K_{sb} and for a uniform quasi-steady ice thinning rate $\partial H_i/\partial t = -1$ m yr^{-1}.

thinning rate $\partial H_i/\partial t < 0$. Because the compaction terms vanish in a steady state, we consider a quasi-steady state in which all other time derivatives are zero, and the ice thinning is assumed to have a negligible effect on the topographic terms. The ice thinning increases vertical groundwater flux in the upwards direction, enhancing the heat flux relative to the case with $S_S = 0$. The enhancement to the heat flux again scales with S_S (*i.e.* with Σ). Because the compaction-driven part of the groundwater flow scales with the sedimentary basin thickness H_{sb}, the overall heat flux enhancement is largest where the sedimentary basin is thickest.

A further 2D example solution, including more variation in the sedimentary basin geometry and a nonuniform geothermal heat flux, is shown in Appendix C.

4. ASYMPTOTIC SOLUTION FOR SMALL PÉCLET NUMBER

Realistic values of the hydraulic conductivity suggest the Péclet number of the sedimentary basin is relatively small. In particular, Gooch and others (2016) and Robel and others (2023) consider a range of permeabilities equivalent to $K_{sb} = 10^{-10}$–10^{-6} ms^{-1}, giving Pe between 3×10^{-6} and 0.03. It therefore makes sense to consider the behaviour of the problem when Pe is asymptotically small. In the following calculation, we ignore the radiogenic heating $\hat{Q}_r$ for simplicity, although the result can easily be generalised to include $\hat{Q}_r$. We also neglect dissipative heating, which is justified provided that the parameter Ξ_{sb} is small.

In the limit Pe = 0, the temperature profile is simply given by

$$\hat{T}_{sb} = \hat{T}_0 := \hat{G}(\hat{b} - \hat{z}), \tag{29}$$

so that the heat flux at the ice-bed interface is just the geothermal heat $\hat{G}$, with no perturbation due to groundwater flow. For small but nonzero Pe, we expand $\hat{T}_{sb}$ as an asymptotic series

$$\hat{T}_{sb} \sim \hat{T}_0 + \mathrm{Pe}\hat{T}_1 + \dots \tag{30}$$

At leading order $\hat{T}_0$ is as above, and at first order we have (from Equation (24), assuming a quasi-steady state, *i.e.* $\partial T_{sb}/\partial t = 0$, and that Ξ_{sb} is negligibly small)

$$\frac{\partial^2 \hat{T}_1}{\partial \hat{z}^2} = \hat{\mathbf{u}}_{\mathbf{sb}} \cdot \hat{\nabla}\hat{T}_0 + \hat{w}_{sb}\frac{\partial \hat{T}_0}{\partial \hat{z}}. \tag{31}$$

For Peer Review

Substituting in the Darcy flux components given by Equation (23) and $\hat{T}_0$, we have

$$\frac{\partial^2 \hat{T}_1}{\partial \hat{z}^2} = -\hat{\nabla}\hat{\psi} \cdot ((\hat{b} - \hat{z})\hat{\nabla}\hat{G} + \hat{G}\hat{\nabla}\hat{b}) - \left((\hat{z} - \hat{b} + \hat{H}_{sb})\left(\hat{\nabla}^2\hat{\psi} - \frac{\Sigma}{\kappa}\frac{\partial \hat{\psi}}{\partial \hat{t}}\right) - \hat{\nabla}\hat{\psi} \cdot \hat{\nabla}(\hat{b} - \hat{H}_{sb})\right)\hat{G}. \tag{32}$$

After simplifying and integrating, we find

$$\frac{\partial \hat{T}_1}{\partial \hat{z}} = \frac{1}{2}\left((\hat{z} - \hat{b})^2 - \hat{H}_{sb}^2\right)\hat{\nabla}\hat{\psi} \cdot \hat{\nabla}\hat{G} - (\hat{z} - \hat{b} + \hat{H}_{sb})\hat{G}\left(\hat{\nabla}\hat{\psi} \cdot \hat{\nabla}\hat{H}_{sb}\right) + \frac{1}{2}(\hat{z} - \hat{b} + \hat{H}_{sb})^2\hat{G}\left(\hat{\nabla}^2\hat{\psi} - \frac{\Sigma}{\kappa}\frac{\partial \hat{\psi}}{\partial \hat{t}}\right). \tag{33}$$

Evaluating at the surface, we find after further simplifying that

$$-\left.\frac{\partial \hat{T}_1}{\partial \hat{z}}\right|_{\hat{z}=\hat{b}} = \hat{\nabla} \cdot \left(\frac{1}{2}\hat{G}\hat{H}_{sb}^2\hat{\nabla}\hat{\psi}\right) - \frac{1}{2}\frac{\Sigma}{\kappa}\hat{G}\hat{H}_{sb}^2\frac{\partial \hat{\psi}}{\partial \hat{t}}, \tag{34}$$

where we have terms originating from the topographically-driven (involving $\nabla\psi$) and compaction-driven (involving $\partial\psi/\partial t$) groundwater flow respectively, similarly to the exfiltration q_E (Equation (19)). In dimensional variables, we have that

$$-k_{sb}\left.\frac{\partial T}{\partial z}\right|_{z=b} \sim G + \frac{\rho_w c_w}{k_{sb}}\left(\nabla \cdot \left(\frac{1}{2}K_{sb}G{H_{sb}}^2\nabla\psi\right) - \frac{1}{2}S_S(1-\xi)GH_{sb}^2\frac{\partial \psi}{\partial t}\right). \tag{35}$$

This heat flux modification results in a modification Δm to the melt rate at the ice bed. Specifically, defining the unperturbed melt rate as

$$m_0 = \frac{1}{\rho_w L}\left(G + k_i\frac{\partial T_i}{\partial z} + \tau_{\mathbf{b}} \cdot \mathbf{u_b} + D_h\right), \tag{36}$$

Equation (15) gives that

$$m = m_0 + \Delta m, \quad \Delta m = \frac{c_w}{k_{sb}L}\left(\nabla \cdot \left(\frac{1}{2}K_{sb}G{H_{sb}}^2\nabla\psi\right) - \frac{1}{2}S_S(1-\xi)GH_{sb}^2\frac{\partial \psi}{\partial t}\right). \tag{37}$$

We test the asymptotic approximation (34) using the 2D example previously shown in Figure 3, in order to determine the scope of its validity. The results are shown in Figure 4. Figure 4(a) shows the performance of the asymptotic approximation for various hydraulic conductivities K_{sb} and hence Péclet numbers Pe. The asymptotic approximation fits the numerical solution very well for $K_{sb} = 1 \times 10^6$ (Pe = 0.0047), but

For Peer Review

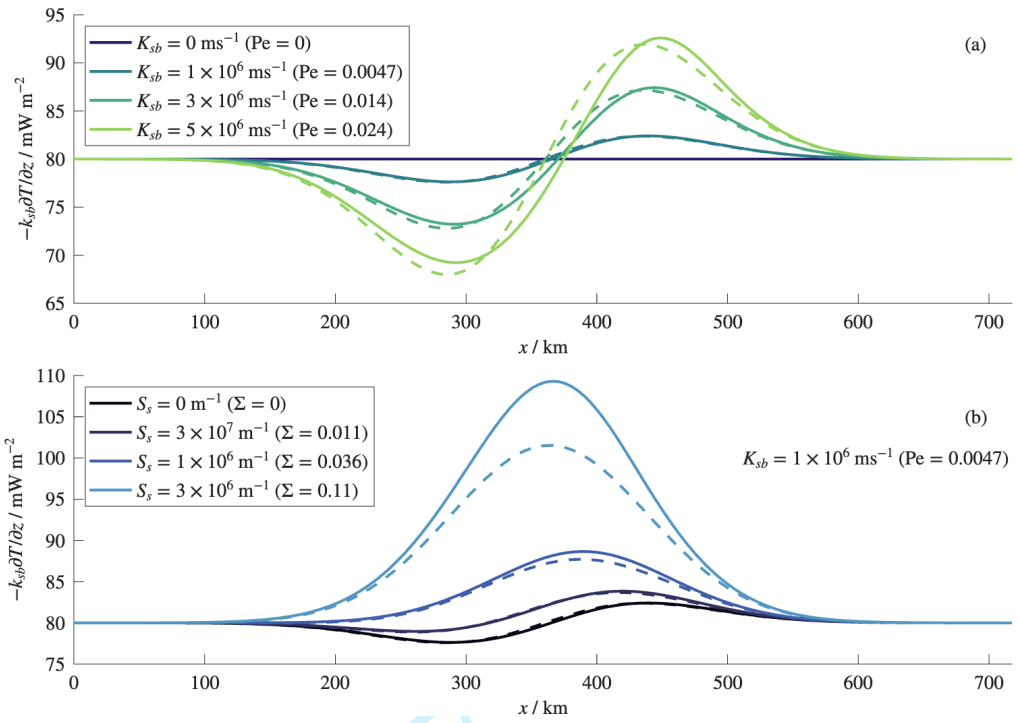

Fig. 4. Comparison of asymptotic solution (dashed line) with the numerical solution (solid line), for the example shown in Figure 3. (a) tests the asymptotic solution for varying K_{sb} / Pe, whereas (b) tests the asymptotic solution for varying S_S / Σ and a fixed value of K_{sb}.

begins to deviate from the numerical solution for Pe > 0.01. The Péclet number at which the solutions differ noticeably will vary slightly depending on specifics of the problem such as H_{sb}, G, and the hydraulic gradient.

In Figure 4(b), the asymptotic solution is compared to the numerical solution for different values of the specific storage S_S, leading to different values of Σ, with a fixed K_{sb}. This time, the approximation agrees well with the numerical solution up to and including $\Sigma = 0.036$, but for $\Sigma = 0.11$ the asymptotic approximation underestimates the perturbation to the flux. This means that, as well as small Pe being small, this approximation also requires small Σ in order to be accurate, so that the compaction-driven contribution to the groundwater flow is not too large. Taken together, these results suggest that Equation (34) is a reliable approximation to the solution of the heat equation (24), provided that K_{sb} and S_S are not too large. In Appendix C, we test this approximation against the numerical solution for a different case including more complex sedimentary basin geometry and a nonuniform G, in order to obtain further evidence for the reliability of the approximate solution in a more general case.

Peer Review

5. APPLICATION TO ANTARCTIC DATA

The approximate expression (34) for the heat flux modification for small Péclet number is useful insofar that it enables an approximate calculation of the effect of groundwater flow on subglacial heating without needing to solve a PDE. We can therefore evaluate this expression using estimated subglacial heat flux and sedimentary basin thickness from Antarctica. When estimating the heat flux modification by groundwater beneath Antarctica, the main source of uncertainty comes from the values of K_{sb} and S_S. We take these as constant in space for simplicity and work with large but realistic values, while noting that the topographically-driven and compaction-driven terms scale linearly with K_{sb} and S_S respectively.

For simplicity, we continue to parametrise the effective pressure as 10% of the overpressure ($N = 0.1\rho_i g H_i$). We also assume a thawed bed everywhere, although we note that significant regions of Antarctica are likely to have a frozen bed. We designate by hatching the regions where the bed is likely to be frozen (Seiner and others, 2025), in which our results are less likely to be reliable.

In this section, we use the geothermal heat flux model of Stål and others (2021) and the sedimentary basin thickness from Li and others (2022), both of which have 20-kilometer resolution. We use this geothermal heat flux model as the prescribed heat flux at the base of the sedimentary basin, and therefore neglect radiogenic heat production in the sedimentary basin. The compaction component uses the ice thickness rate of change $\partial H_i/\partial t$ (assumed steady) from ICESAT satellite data (Smith and others, 2020). The coverage excludes a region around the South pole, which we denote with a dashed circle, and in which we assume $\partial H_i/\partial t = 0$. A plot of this data is provided in Appendix C, Figure 11. We use ice thickness H_i and bed elevation b data from Bedmap3 (Pritchard and others, 2025).

5.1 Heat flux modification

Figure 5 shows the result of applying the asymptotic solution for the heat flux modification for values $K_{sb} = 10^{-6}$ m s^{-1} and $S_S = 10^{-5}$ m^{-1}. These values correspond to Pe $= 3.3 \times 10^{-3}$ or $\kappa = 8.6 \times 10^{-3}$ and to $\Sigma = 0.073$. Despite the small Péclet number, we can see that the asymptotic solution predicts that geothermal heat can be modified by tens of mW m^{-2} in either direction, representing a substantial modification, for these large but realistic parameter values. We first discuss the compaction term, before examining the topographic term region by region.

Due to the high ice thinning rates beneath Pine Island and Thwaites glaciers (PIG and TG), the effect of

For Peer Review

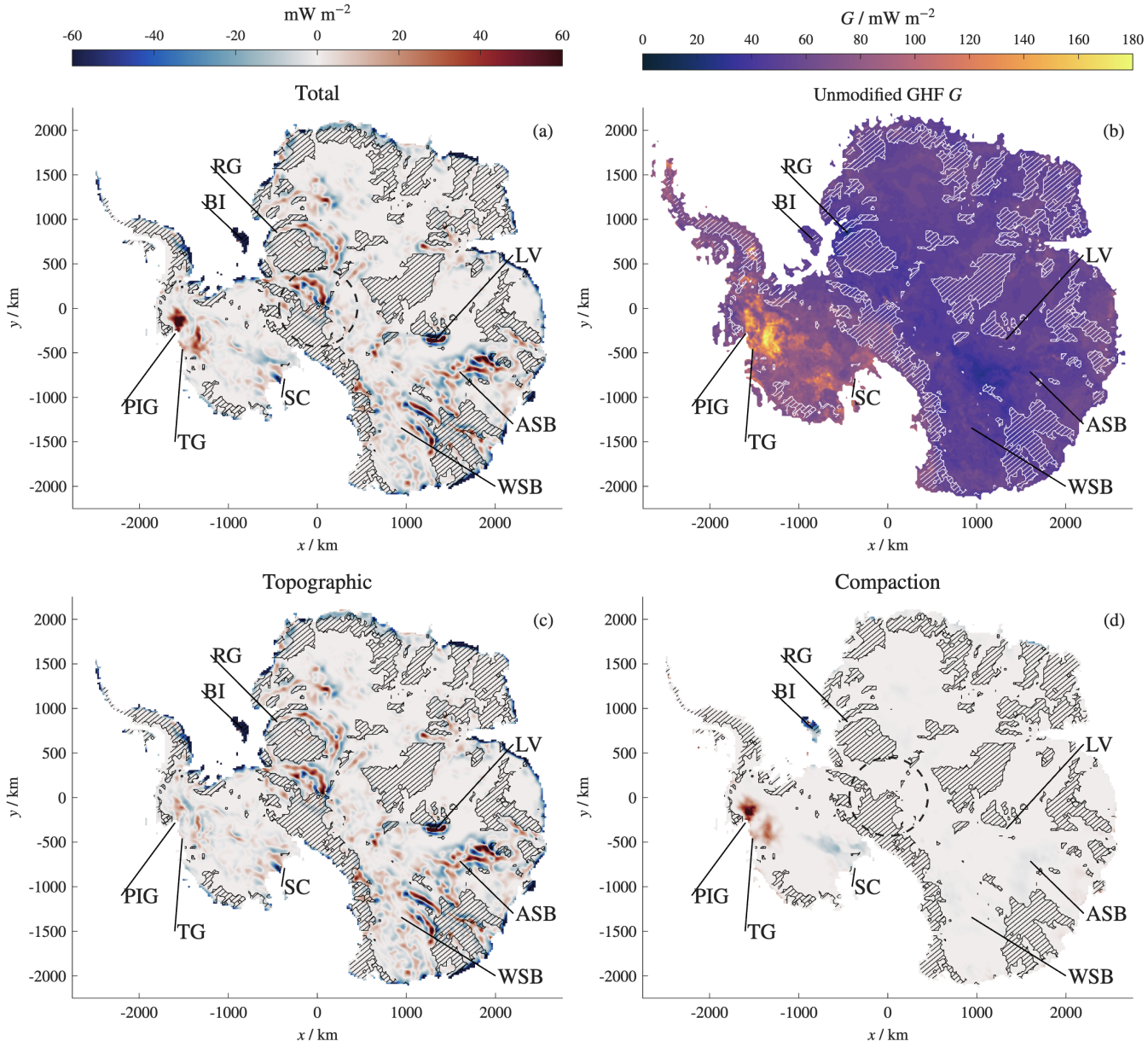

Fig. 5. Geothermal heat flux modification (34) for $K_{sb} = 10^{-6}$ m s^{-1} and $S_S = 10^{-5}$ m^{-1}. Panel (a) shows the total modification, compared to the unmodified heat flux G in (b). (c) shows the topographic term and (d) the compaction term. Selected locations are marked by abbreviations. The dashed circle around the South pole marks a gap in the thinning rate data, wherein we assume $\partial H_i/\partial t = 0$. Hatched regions denote regions where the bed is likely frozen (Seiner and others, 2025).

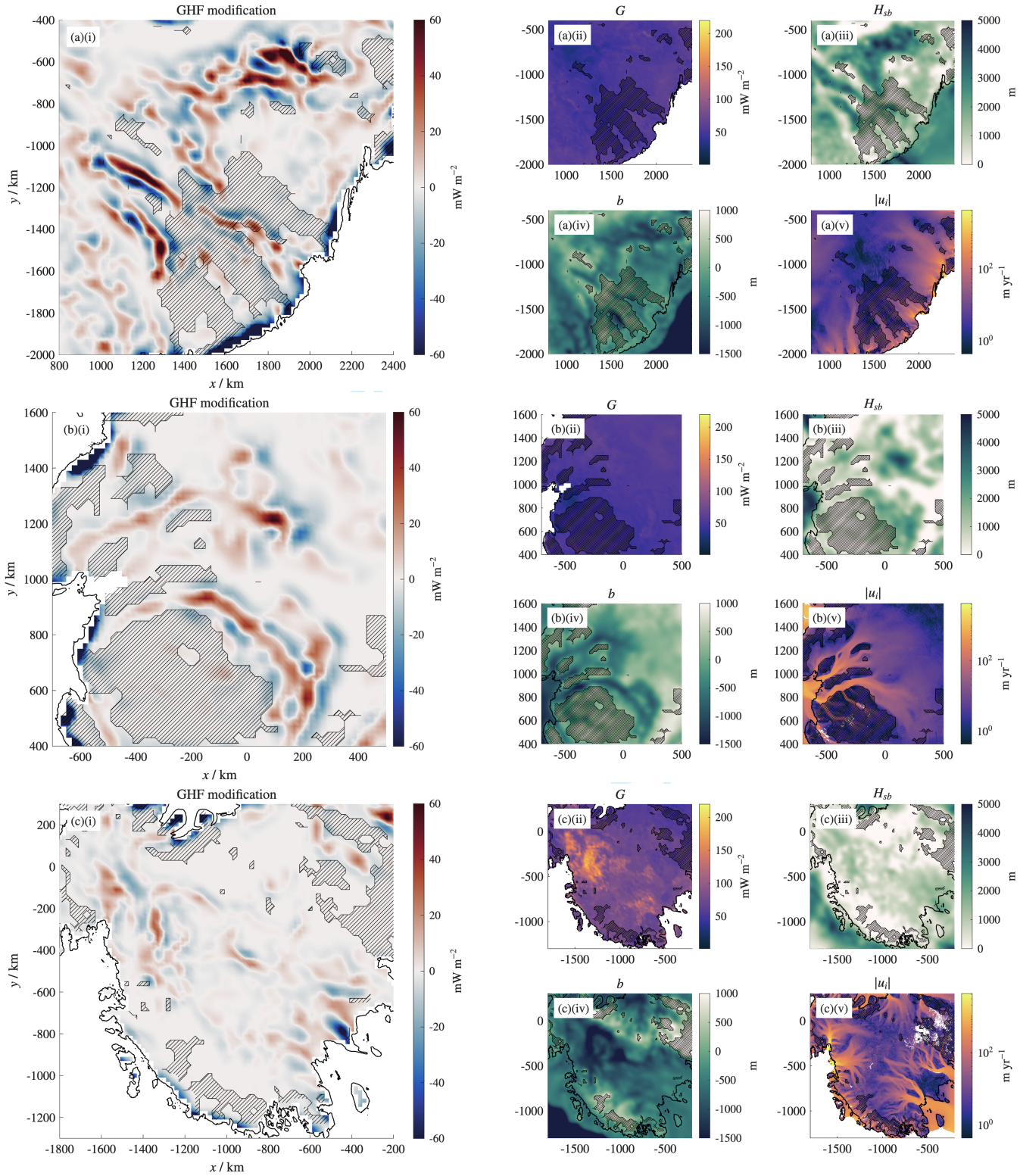

Fig. 6. (i) Zoomed-in regions of the topographic heat flux modification, compared with (ii) the geothermal heat G, (iii), the ice bed topography b, (iv) the hydraulic gradient ψ, and (v) the ice velocity (Mouginot and others, 2017). The regions respectively cover Wilkes subglacial basin (WSB) and Aurora subglacial basin (ASB) (a), and Recovery glacier (RG) (b), both in East Antarctica, and the majority of West Antarctica (c).

compaction-driven groundwater flow is strongest here (Figure 5(d)). The ice thinning drives groundwater flow vertically upwards, which results in a further enhancement of heat flux from its already high value. This compaction-driven enhancement of heat flux in response to ice thinning could act as a positive feedback mechanism that accelerates basal melting, leading to further sliding and ice loss. Conversely, however, this feedback could help to reduce ice flow in regions where the ice is thickening, leading to heat flux reduction by groundwater infiltration. This predicted effect is most visible beneath the stagnated Kamb ice stream on the Siple Coast (SC), which is currently undergoing thickening.

The topographic component (Figure 5(c)) includes a thin region of significant heat flux reduction around the grounding line, particularly in East Antarctica. This is because the sedimentary basin underlies most of the ocean, meaning that a steep increase in sedimentary basin thickness occurs around the grounding line. However, the extent of the sedimentary basin beyond the grounding line may be uncertain and depend on how the data has been processed. Moreover, certain assumptions of the model are likely to break down within a few kilometers of the grounding line: in particular, the effective pressure N may become comparable to the overburden as the ice approaches flotation, and groundwater flow may be influenced by seawater intrusion into the sedimentary basin (Cairns and others, 2025).

A dramatic effect is also seen around Lake Vostok (LV) in East Antarctica, where there is a significant topographic minimum. In addition, substantial geothermal cooling is seen beneath Berkner island (BI) in the Filchner-Ronne ice shelf, where the sedimentary basin is thought to be extremely deep. In these regions, the predicted groundwater flow velocities are large, meaning that the small Péclet number approximation may not be accurate.

Setting aside these uncertain regions, the topographic component of the groundwater flow has a noticeable effect across both East and West Antarctica, which can be seen in more detail in the zoomed-in regions of Figure 6. In East Antarctica, where the heat flux is relatively low, the groundwater-induced effect is strongest beneath Wilkes subglacial basin (WSB) and Aurora subglacial basin (ASB) (Figure 6(a)), because this region includes the deepest sedimentary basins in Antarctica. These sedimentary basins form bands roughly parallel to the ice flow, corresponding to topographic lows in the ice bed, and to the location of ice streams. Topographic highs have little to no sedimentary basin coverage, and in many cases correspond regions where the bed is predicted to be frozen. Beneath Recovery glacier (RG) and the surrounding land (Figure 6(b)), the distinction is even clearer between sedimentary basins below fast-flowing ice in topographic lows and topographic highs with a frozen bed and little sedimentary basin coverage.

For Peer Review

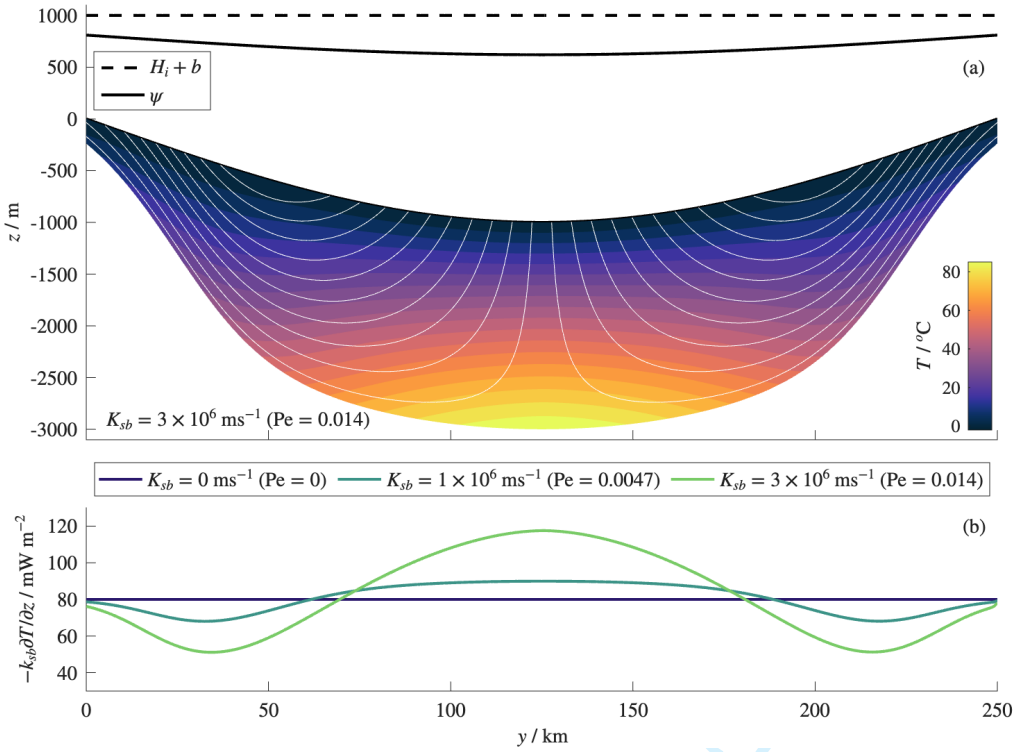

Fig. 7. Numerical solution for an idealised cross-section of an ice stream. The topography is given by $b(y) = -1000\sin(\pi y/250\text{km})$ m, the ice thickness by $H_i(y) = 1000\text{m} - b(y)$, and the sedimentary basin depth $H_{sb}(y) = 1000(1 + \tanh\big((x - 25\text{km})/25\text{km}\big)\tanh\big((225\text{km} - x)/25\text{km}\big))$ m. The heat flux is uniformly given by $G = 80$ mW m^{-2}, we take $N = 0.1\rho_i g H_i$ as elsewhere, and there is no thinning rate of the ice ($\partial H_i/\partial t = 0$). Panel (a) shows the geometry, streamlines of the groundwater flow in white, and temperature at 5°C contours for a particular K_{sb}. Panel (b) compares the heat flux through the top of the sedimentary basin for various K_{sb}.

In both cases, the variations in bed elevation produce a variation in the hydraulic potential (because the ice surface $H_i + b$ is relatively flat). This hydraulic gradient drives a groundwater flow, which results in heat flux enhancement in the centre of the ice stream and reduction at the margins. Such heat flux enhancement via groundwater flow could therefore act as a self-reinforcing mechanism for ice streams, which naturally create sedimentary basins in topographic lows over time by erosion and deposition. Once a sedimentary basin is in place, groundwater flow helps transport heat to the bed of the ice stream and away from its surroundings, making it more likely that the central bed will remain thawed and the surrounding bed remain frozen.

This mechanism is illustrated in Figure 7 by another example solution to the model for a cross-section of an idealised ice stream, which shows the numerical solution of the full problem rather than the asymptotic solution. The topography includes a trough corresponding to the centre of the ice stream. Although the ice surface is uniform, the density difference between ice and water (along with the effective pressure) leads to a non-uniform hydraulic potential, which is lowest in the middle of the ice stream. Groundwater infiltrates near the margins of the ice streams driven by the thickening of the sedimentary basin towards the centre, but exfiltrates in the centre due to the shallowing of the hydraulic gradient. As predicted, this leads to heat flux enhancement in the centre of the ice stream and reduction at the margins, with amplitude up to 40 mW m^{-2} for $K_{sb} = 3 \times 10^{-6}$ m s^{-1} and around 10 mW m^{-2} for $K_{sb} = 1 \times 10^{-6}$ m s^{-1}.

In West Antarctica, a similar banded pattern of heat enhancement in the centre of ice streams and reduction at their margins can be seen along the Siple Coast (SC) (Figure 6(c)). In this case, the variation in bed topography is less than the aforementioned locations in East Antarctica, but the background geothermal heat flux is larger and more important in determining the location of ice streams. The highest heat flux is found beneath Pine Island and Thwaites glacier (PIG and TG), which also comprise the fastest-thinning regions of the grounded Antarctic ice sheet. Similar bands of heating and cooling are seen beneath these glaciers, but alternate in the direction of ice flow rather than transversely.

5.2 Basal melt modification correlates with exfiltration

Assuming a thawed bed, modification of the geothermal heat flux results in a corresponding modification of the basal melt rate. Figure 8(a) shows the resulting modification Δm in the melt rate from the estimated heat flux modification in Figure 5, obtained using Equation (37). For the same parameter values, Figure 8(b) shows the exfiltration q_E, obtained using Equation (19). From a visual inspection Δm and

For Peer Review

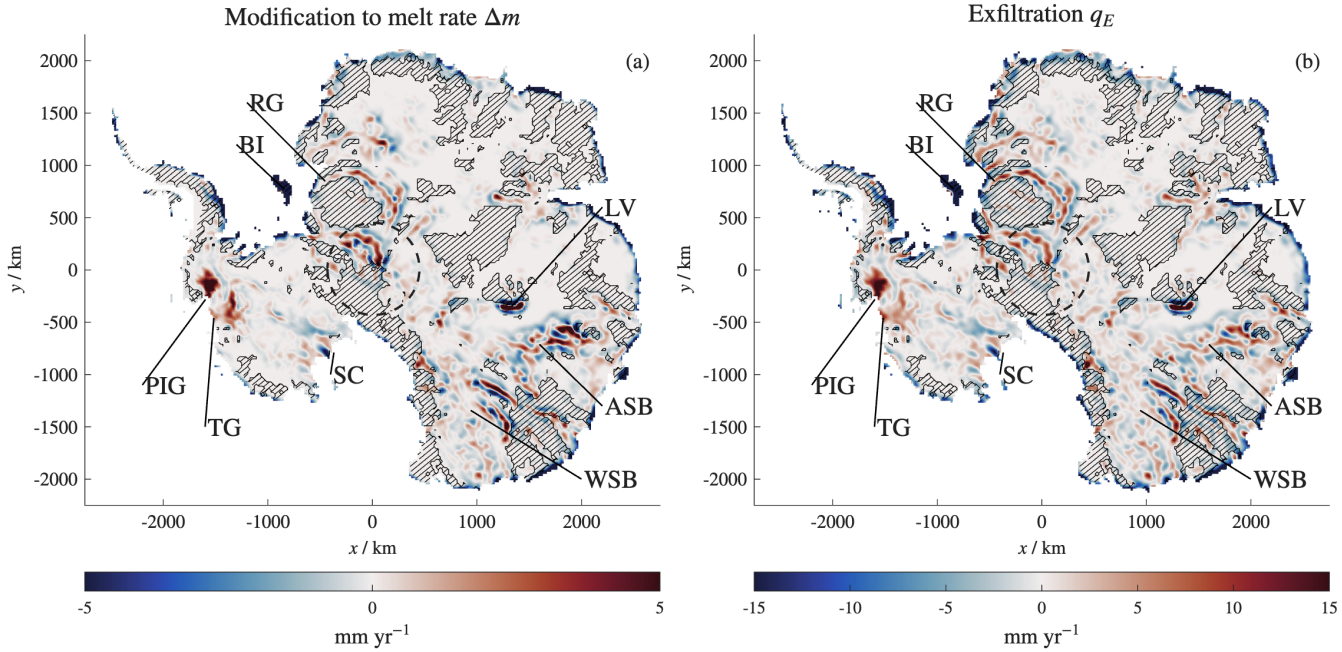

Fig. 8. (a) Asymptotic modification to melt rate based on the heat flux modification above, compared with (b) the exfiltration q_E, for the K_{sb} and S_S in Figure 5.

q_E are closely correlated, but q_E is 2–3 times larger. This suggests that the leading-order contribution of groundwater to subglacial water budgets is through exfiltration and infiltration, but that the modification to the melt rate through geothermal heat flux modification is also significant.

The correlation between Δm and q_E can be understood by referring to Equations (19) and (37), which are almost identical except that the factor H_{sb} in the former is replaced with $\mathrm{St}\hat{G}H_{sb}/2$ in the latter. Converting to dimensional variables, this suggests that the size of the melt modification relative to the exfiltration roughly scales with the parameter $\Lambda = c_p G H_{sb}/k_{sb}L$. This has the form of a Stefan number, where GH_{sb}/k_{sb} is the natural scale for the change in temperature across the depth of the basin.

The parameter Λ is highest where the heat flux is high, such as beneath Pine Island and Thwaites glaciers (PIG and TG), and where the sedimentary basins are thickest, such as beneath Wilkes and Aurora subglacial basins (WSB and ASB). In these locations, the melt rate modification Δm in Figure 8(a) contributes a relatively large portion of the water budget. A plot of Λ is provided in Appendix C, Figure 12.

For Peer Review

6. DISCUSSION

In this paper we have described a simple model for three-dimensional heat transport and groundwater flow in a sedimentary basin, including both topography and compaction as drivers of flow. This model predicts that heat flux is typically enhanced where groundwater is exfiltrated and reduced where groundwater infiltrates. We have derived an asymptotic approximation for the modification to the groundwater flux for small Péclet numbers, and shown that this approximates the numerical solution well for realistic parameter values.

We find that, for large but realistic parameter values, the heat flux beneath Antarctica could be modified by tens of mW m^{-2} in either direction, representing a significant alteration. This highlights the need to account for groundwater flow in models of Antarctic geothermal heat flux. Topographically-driven groundwater flow tends to enhance heat flux in topographic lows at the centre of glaciers, and reduce heat flux at the margins, providing a potential self-reinforcing mechanism for ice streams across much of both West and East Antarctica. Compaction-driven groundwater flow also provides a potential positive feedback by enhancing heat flux below ice that is already thinning, an effect that is currently concentrated beneath Thwaites and Pine Island glaciers.

We have made a number of simplifying assumptions in order to obtain these results. First is our use of an asymptotic solution for the heat flux modification in Section 5 (rather than the full solution of the equations). This asymptotic solution may prove inaccurate when groundwater fluxes are large, and in particular may underestimate the magnitude of the perturbation. However, this approximation is unlikely to substantially affect the qualitative behaviour, and likely has less impact than other assumptions.

Another assumption is that of an isothermal thawed bed, when in reality large regions of the Antarctic bed are likely to be frozen. Where the bed is frozen, the permeability of the frozen rock is reduced to almost zero. Modelling of this region would require introducing a free boundary representing the extent of the frozen region, whose position is determined by balances of energy and water mass across the boundary. It can be noted (referring to Figure 1(b)) that the overlap of sedimentary basins with frozen bed regions is small, partly because sedimentary basins are formed by the deposition of sediments in topographic lows, whereas the bed is more likely to be frozen in topographic highs. This suggest that we need not be concerned with bed freezing over many of our smaller-scale regions of interest, although there are some exceptions *e.g.* in Wilkes Land and near the South Pole.

For Peer Review

Our treatment of the basal temperature overlaps with our simplifying assumptions about the basal effective pressure, which we have parameterised in a simple way. This allows us to avoid solving a PDE (or system of PDEs) to describe the subglacial drainage system. A flotation fraction of 90% (as we have assumed) is a reasonable value for most of Antarctica, but near the grounding line in particular the flotation fraction is likely to be significantly higher (Ehrenfeucht and others, 2025). This suggests that our modelling overestimates the hydraulic potential gradient, and thus the groundwater fluxes, in this region. The work in this paper could be developed by including a simple coupled model of subglacial hydrology (*e.g.* Kazmierczak and others, 2024; Cairns and others, 2026), or by incorporating the effect of groundwater flow into a more involved hydrology model (*e.g.* GlaDS (Werder and others, 2013) or SHAKTI (Sommers and others, 2018)).

We have also only considered steady- or quasi-steady-state models. In reality, grounding line motion and ice thickness changes will introduce transience into the groundwater flow over timescales of centuries to millenia. Evolution of the subglacial hydrological system will also induce changes in the effective pressure over much faster timescales of months to years. While exploring time-dependent solutions is beyond the scope of this paper, it could provide further insight into the feedbacks associated with ice streams and ice thinning suggested by our results above. In addition, the slow response time of groundwater in sedimentary basins could mean that groundwater flow and thus temperature profiles in sedimentary basins are still responding to historic ice sheet changes, rather than being in a steady state (Cairns and others, 2025).

Outside of our modelling assumptions, our work is also limited by current knowledge of the geology and hydraulic properties of sedimentary basins. We have assumed a spatially uniform hydraulic conductivity in our calculations, although the permeability and hence conductivity of sedimentary basins is likely to be highly heterogeneous even on small scales. For instance, faults could act as highly localised regions of high permeability, concentrating groundwater flow and hence heat flux enhancement (Tankersley and others, 2022). Until the hydraulic properties of sedimentary basins are better known, our work can provide at best an order-of-magnitude estimate of the importance of groundwater and a qualitative description of its likely behaviour.

All in all, however, our work expands the existing scientific framework for modelling the effect of groundwater flow on Antarctic geothermal heat flux, and demonstrates the need for further investigation into this topic. The development of more complex mathematical models, alongside further advances in

For Peer Review

using geophysical methods to investigate Antarctic sedimentary basins, will enable future breakthroughs in understanding the basal conditions of Antarctica and the future of the Antarctic ice sheet.

CODE AVAILABILITY

Code used to generate the figures in this paper is available at https://doi.org/10.5281/zenodo.20646472.

REFERENCES

Aitken ARA, Li L, Kulessa B, Schroeder D, Jordan TA, Whittaker JM, Anandakrishnan S, Dawson EJ, Wiens DA, Eisen O and Siegert MJ (2023) Antarctic sedimentary basins and their influence on ice-sheet dynamics. *Reviews of Geophysics*, **61**(3), e2021RG000767 (doi: https://doi.org/10.1029/2021RG000767), e2021RG000767 2021RG000767

Bear J (2013) *Dynamics of fluids in porous media*. Courier Corporation, ISBN 978-0-486-65675-5

Burton-Johnson A, Dziadek R and Martin C (2020) Geothermal heat flow in Antarctica: Current and future directions. *The Cryosphere Discussions*, **2020**, 1–45

Cairns G, Benham G and Hewitt I (2025) Groundwater dynamics beneath a marine ice sheet. *The Cryosphere*, **19**(9), 3725–3747

Cairns GJ, Benham GP and Hewitt IJ (2026) Groundwater feedbacks on ice sheets and subglacial hydrology [preprint]. *arXiv preprint arXiv:2602.14905*

Christoffersen P and Tulaczyk S (2003) Thermodynamics of basal freeze-on: predicting basal and subglacial signatures of stopped ice streams and interstream ridges. *Annals of Glaciology*, **36**, 233–243

Dawson EJ, Schroeder DM, Chu W, Mantelli E and Seroussi H (2022) Ice mass loss sensitivity to the Antarctic ice sheet basal thermal state. *Nature Communications*, **13**(1), 4957

Ehrenfeucht S, Dow C, McArthur K, Morlighem M and McCormack F (2025) Antarctic wide subglacial hydrology modeling. *Geophysical Research Letters*, **52**(1), e2024GL111386

Flowers G (2015) Modelling water flow under glaciers and ice sheets. *Proceedings of the Royal Society A: Mathematical, Physical and Engineering Sciences*, **471**(2176), 20140907

Gooch B, Young D and Blankenship D (2016) Potential groundwater and heterogeneous heat source contributions to ice sheet dynamics in critical submarine basins of East Antarctica. *Geochemistry, Geophysics, Geosystems*, **17**(2), 395–409

For Peer Review

Gregov T, Pattyn F and Arnst M (2023) Grounding-line flux conditions for marine ice-sheet systems under effective-pressure-dependent and hybrid friction laws. *Journal of Fluid Mechanics*, **975**, A6

Gustafson C, Key K, Siegfried M, Winberry J, Fricker H, Venturelli R and Michaud A (2022) A dynamic saline groundwater system mapped beneath an Antarctic ice stream. *Science*, **376**(6593), 640–644

Kazmierczak E, Gregov T, Coulon V and Pattyn F (2024) A fast and unified subglacial hydrological model applied to Thwaites Glacier, Antarctica. *EGUsphere*, **2024**, 1–36

Li L and Aitken A (2024) Crustal heterogeneity of Antarctica signals spatially variable radiogenic heat production. *Geophysical Research Letters*, **51**(2), e2023GL106201 (doi: https://doi.org/10.1029/2023GL106201), e2023GL106201 2023GL106201

Li L, Aitken A, Lindsay M and Kulessa B (2022) Sedimentary basins reduce stability of antarctic ice streams through groundwater feedbacks. *Nature Geoscience*, **15**(8), 645–650

MacAyeal D (1989) Large-scale ice flow over a viscous basal sediment: Theory and application to ice stream B, Antarctica. *Journal of Geophysical Research: Solid Earth*, **94**(B4), 4071–4087

McCormack F, Roberts J, Dow C, Stål T, Halpin J, Reading A and Siegert M (2022) Fine-scale geothermal heat flow in Antarctica can increase simulated subglacial melt estimates. *Geophysical Research Letters*, **49**(15), e2022GL098539 (doi: DOI.org/10.1029/2022GL098539)

Mouginot J, Scheuchl B and Rignot E (2017) MEaSUREs Antarctic boundaries for IPY 2007-2009 from satellite radar, version 2 (doi: 10.5067/AXE4121732AD)

Muszynski I and Birchfield G (1987) A coupled marine ice-stream–ice-shelf model. *Journal of Glaciology*, **33**(113), 3–15

Pittard M, Galton-Fenzi B, Roberts J and Watson C (2016) Organization of ice flow by localized regions of elevated geothermal heat flux. *Geophysical Research Letters*, **43**(7), 3342–3350

Pritchard HD, Fretwell PT, Fremand AC, Bodart JA, Kirkham JD, Aitken A, Bamber J, Bell R, Bianchi C, Bingham RG, Blankenship DD, Casassa G, Christianson K, Conway H, Corr HFJ, Cui X, Damaske D, Damm V, Dorschel B, Drews R, Eagles G, Eisen O, Eisermann H, Ferraccioli F, Field E, Forsberg R, Franke S, Goel V, Gogineni SP, Greenbaum J, Hills B, Hindmarsh RCA, Hoffman AO, Holschuh N, Holt JW, Humbert A, Jacobel RW, Jansen D, Jenkins A, Jokat W, Jong L, Jordan TA, King EC, Kohler J, Krabill W, Maton J, Gillespie MK, Langley K, Lee J, Leitchenkov G, Leuschen C, Luyendyk B, MacGregor JA, MacKie E, Moholdt G, Matsuoka K, Morlighem M, Mouginot J, Nitsche FO, Nost OA, Paden J, Pattyn F, Popov S, Rignot E, Rippin DM, Rivera A, Roberts JL, Ross N, Ruppel A, Schroeder DM, Siegert MJ, Smith AM, Steinhage D, Studinger M, Sun B, Tabacco I, Tinto

For Peer Review

KJ, Urbini S, Vaughan DG, Wilson DS, Young DA and Zirizzotti A (2025) Bedmap3 updated ice bed, surface and thickness gridded datasets for Antarctica. *Scientific data*, **12**(1), 414 (doi: 10.1038/s41597-025-04672-y)

Reading AM, Stål T, Halpin JA, Lösing M, Ebbing J, Shen W, McCormack FS, Siddoway CS and Hasterok D (2022) Antarctic geothermal heat flow and its implications for tectonics and ice sheets. *Nature Reviews Earth & Environment*, **3**(12), 814–831

Robel A, Sim S, Meyer C, Siegfried M and Gustafson C (2023) Contemporary ice sheet thinning drives subglacial groundwater exfiltration with potential feedbacks on glacier flow. *Science Advances*, **9**(33), eadh3693

Schoof C (2007) Ice sheet grounding line dynamics: Steady states, stability, and hysteresis. *Journal of Geophysical Research: Earth Surface*, **112**(F3)

Seiner O, Hugney A, Seroussi H and MacGregor JA (2025) A synthesis of the basal thermal state of the Antarctic ice sheet. *Journal of Glaciology*, 1–30

Seroussi H, Nowicki S, Payne AJ, Goelzer H, Lipscomb WH, Abe-Ouchi A, Agosta C, Albrecht T, Asay-Davis X, Barthel A, Calov R, Cullather R, Dumas C, Galton-Fenzi BK, Gladstone R, Golledge NR, Gregory JM, Greve R, Hattermann T, Hoffman MJ, Humbert A, Huybrechts P, Jourdain NC, Kleiner T, Larour E, Leguy GR, Lowry DP, Little CM, Morlighem M, Pattyn F, Pelle T, Price SF, Quiquet A, Reese R, Schlegel NJ, Shepherd A, Simon E, Smith RS, Straneo F, Sun S, Trusel LD, Van Breedam J, van de Wal RSW, Winkelmann R, Zhao C, Zhang T and Zwinger T (2024) Evolution of the Antarctic ice sheet over the next three centuries from an ISMIP6 model ensemble. *Earth's Future*, **12**(9), e2024EF004561 (doi: https://DOI.org/10.1029/2024EF004561)

Smith B, Fricker HA, Gardner AS, Medley B, Nilsson J, Paolo FS, Holschuh N, Adusumilli S, Brunt K, Csatho B, Harbeck K, Markus T, Neumann T, Siegfried MR and Zwally HJ (2020) Pervasive ice sheet mass loss reflects competing ocean and atmosphere processes. *Science*, **368**(6496), 1239–1242 (doi: 10.1126/science.aaz5845)

Sommers A, Rajaram H and Morlighem M (2018) SHAKTI: Subglacial Hydrology and Kinetic, Transient Interactions v1.0. *Geoscientific Model Development*, **11**(7), 2955–2974 (doi: 10.5194/gmd-11-2955-2018)

Stål T, Reading AM, Halpin JA and Whittaker JM (2021) Antarctic geothermal heat flow model: Aq1. *Geochemistry, Geophysics, Geosystems*, **22**(2), e2020GC009428

Tankersley M, Horgan H, Siddoway C, Caratori Tontini F and Tinto K (2022) Basement topography and sediment thickness beneath Antarctica's Ross ice shelf. *Geophysical Research Letters*, **49**(10), e2021GL097371

Werder M, Hewitt I, Schoof C and Flowers G (2013) Modeling channelized and distributed subglacial drainage in two dimensions. *Journal of Geophysical Research: Earth Surface*, **118**(4), 2140–2158 (doi: https://doi.org/10.1002/jgrf.20146)

For Peer Review

APPENDIX A: ICE SHEET MODEL

For our example two-dimensional solutions in Figures 3 and 9, we use a shallow-shelf ice sheet model with a Weertman sliding law. Noting that in these examples we only consider one horizontal dimension, the thickness $H_i(x,t)$ and horizontal velocity $u_i(x,t)$ (assumed uniform in depth) of the ice obey the mass and momentum equations (Muszynski and Birchfield, 1987; MacAyeal, 1989; Schoof, 2007)

$$\frac{\partial H_i}{\partial t} + \frac{\partial}{\partial x} \cdot (H_i u_i) = a, \tag{A1}$$

$$\frac{\partial}{\partial x}\left(2A^{-1/n} H_i \left|\frac{\partial u_i}{\partial x}\right|^{1/n-1} \frac{\partial u_i}{\partial x}\right) - \beta_W \left|u_i\right|^{m_W - 1} u_i - \rho_i g H_i \frac{\partial}{\partial x}\left(H_i + b\right) = 0, \tag{A2}$$

where $a(x,t)$ is the net accumulation, A is a rheological parameter assumed constant, β_W is a sliding constant, and we take the exponents to be $n = 3$ and $m_W = 1/3$. The boundary conditions are

$$u_i = 0 \quad \text{at} \quad x = 0. \tag{A3}$$

$$\rho_i g H_i = -\rho_w g b \quad \text{at} \quad x = x_g, \tag{A4}$$

$$2A^{-1/n} H_i \left|\frac{\partial u_i}{\partial x}\right|^{1/n-1} \frac{\partial u_i}{\partial x} = \frac{1}{2}\rho_i \left(1 - \frac{\rho_i}{\rho_w}\right) g H_i^2 \quad \text{at} \quad x = x_g. \tag{A5}$$

The first imposes no ice flux at the origin, the second states that the ice achieves flotation at the grounding line, and the third results from balancing the stress required in an unbuttressed ice shelf.

In Figures 3 and 9, we solve these equations for $a = 0.3$ m yr^{-1}, $A = 4.227 \times 10^{-25}$ Pa^{-1} s^3, $\beta_W = 7.624 \times 10^6$ Pa $m^{-1/3}$ $s^{1/3}$, and a topography $b(x) = -100\text{m} - x/2870$.

APPENDIX B: NON-DIMENSIONALISATION

In this Appendix, we describe the choice of scalings used to obtain the dimensionless equations in Section 2.2. We begin by assuming that scales for the accumulation $[a]$, horizontal length $[x]$, and geothermal heat flux $[G]$ are known. We use the vertical lengthscale $[z]$ as a scale for the bed elevation b, the ice thickness H_i, the sedimentary basin thickness H_{sb}, and the hydraulic head ψ. We scale the temperature relative to melting point $T_i - T_m$ with a scale

$$[\Delta T] = [G][z]/k_{sb}. \tag{B1}$$

For Peer Review

Scales for the vertical lengthscale and velocity can either be inferred from data, or found by balancing (motivated by Equations (A1) and (A2))

$$[z][u_i] = [a][x], \quad \beta_W [u_i]^{m_W} = \rho_i g [z]^2/[x]. \tag{B2}$$

The timescale is then given by

$$[t] = [x]/[u_i] = [z]/[a]. \tag{B3}$$

For brevity, we do not include the dimensionless equations (A1) and (A2) for the ice mass and momentum, which may be found in *e.g.* Schoof (2007).

Following Equation (15), we choose a scale for the melt rate based on the heat flux from the sedimentary basin

$$[m] = [G]/\rho_w L. \tag{B4}$$

We also use $[m]$ as the scale for q_E, so that we can straightforwardly compare the two source terms. Darcy's law (8) then provides scales for the groundwater flow components in the sedimentary basin

$$[u_{sb}] = K_{sb}\frac{[z]}{[x]}, \quad [w_{sb}] = \frac{[z]}{[x]}[u_{sb}] = K_{sb}\frac{[z]^2}{[x]^2}. \tag{B5}$$

APPENDIX C: ADDITIONAL FIGURES

In this Appendix, we provide some additional figures to support the main text. In Figure 9, we provide an example 2D steady state solution similar to Figure 3 for a more complex setup. The sedimentary basin includes a bottleneck at $x = 200$ km, driving exfiltration and subsequent infiltration, and reduces in thickness approaching the grounding line, driving further exfiltration. The geothermal heat flux has a local peak at $x = 450$ km and is elsewhere uniform. Figure 9(a) shows the streamlines of this groundwater flow, which advects heat, reducing the thermal gradient where groundwater flows downwards and increasing it when groundwater flows upwards as in Figure 3.

Figure 9(b) shows the resulting modification to the heat flux, with the difference between the modified and unmodified flux approximately scaling with Pe as before. The horizontal component of the groundwater flow also plays a role, as the basal heat flux enhancement from $x = 500$–600 km is magnified by the region of elevated geothermal heat upstream of this region.

For Peer Review

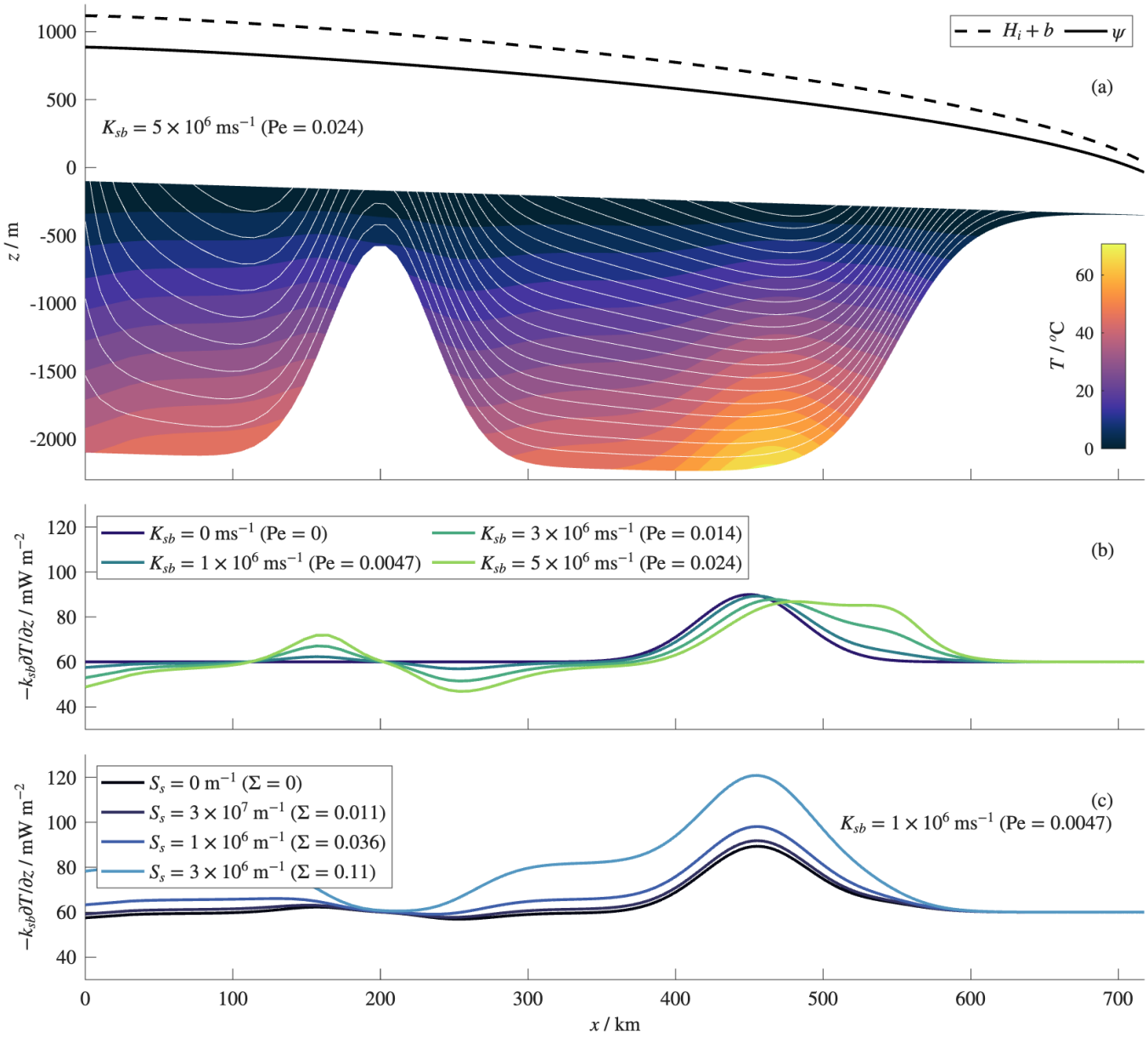

Fig. 9. Steady state solution for a test case with sedimentary basin thickness $H_{sb} = (1000 - 1000\tanh((x - 550\text{km})/50\text{km}) - 1600\exp(-((x - 200\text{km})/50\text{km})^2))$ m, and geothermal heat flux $G = (60 + 30\exp(-((x - 450\text{km})/50\text{km})^2)))$ mW m^{-2}. The effective pressure N is fixed at 10% of the overburden, and the ice thickness is found by solving the shallow-shelf model above. (a) shows the ice profile and hydraulic potential ψ, along with the temperature in the sedimentary basin at 5° contours and streamlines of the groundwater flow for a relatively high hydraulic conductivity K_{sb} with $S_S = 0$. (b) and (c) show the heat flux to the ice bed for various values of K_{sb} with $S_S = 0$, and for various values of the specific storage S_S for a fixed K_{sb} and for a uniform quasi-steady ice thinning rate $\partial H_i/\partial t = -1$ m yr^{-1}.

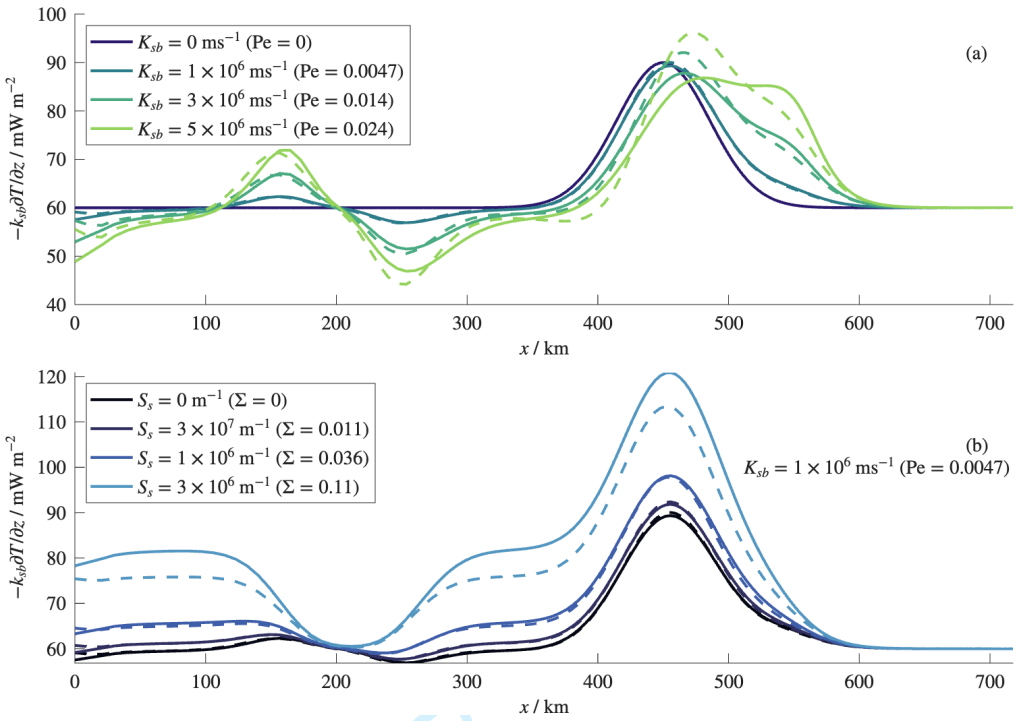

Fig. 10. Comparison of asymptotic solution (dashed line) with the numerical solution (solid line), for the example shown in Figure 9. The heat flux at the ice-bed interface is shown for (a) varying K_{sb} (Pe), and (b) varying S_S (Σ) and a fixed value of K_{sb}.

Peer Review

Figure 9(c) shows the effect of compaction-driven exfiltration, again for a spatially-uniform steady ice thinning rate $\partial H_i/\partial t < 0$ in a quasi-steady state. The ice thinning increases vertical groundwater flux in the upwards direction, enhancing the heat flux by an amount that scales with S_S (*i.e.* with Σ), and is also largest where the sedimentary basin is thickest.

Figure 10, similarly to Figure 4, shows a comparison of the numerical solution for the heat flux with the approximate solution (34), this time for the case in Figure 9. In Figure 10(a), which shows the effect of varying K_{sb} (hence Pe) for $S_S = 0$, we see once more that the approximation matches the numerical solution well roughly for Pe< 0.01, but becomes less accurate for higher values of Pe.

Figure 10(b) shows the effect of varying S_s (hence Σ) for a fixed K_{sb}. Again, the approximate solution agrees well with the numerical solution for Σ up to 0.036, but overestimates the heat flux modification for the higher value $\Sigma = 0.11$. These results provide further support for using Equation (34) to approximate the full solution of the heat equation (24) provided Pe and Σ are sufficiently small, and in particular that this approximation is reliable for a case where G is non-uniform.

We also include two figures providing additional data relevant to Section 4. Figure 11 shows the rate of change of ice thickness $\partial H_i/\partial t$ used to calculate the compaction-driven heat flux modification and

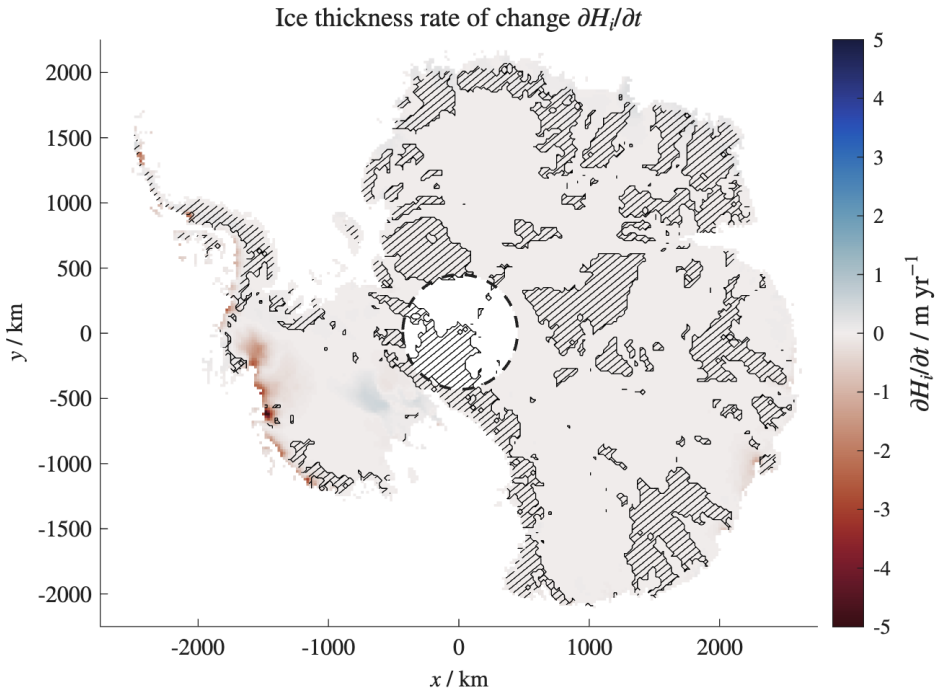

Fig. 11. Data (Smith and others, 2020) for the current rate of change of ice sheet thickness $\partial H_i/\partial t$, used in Section 4. The dashed circle around the South pole indicates a gap in the data.

546 exfiltration for Figures 5 and 8. Figure 12 shows the parameter Λ, which roughly determines the size of
547 the melt rate modification relative to the exfiltration in Figure 8.

Peer Review

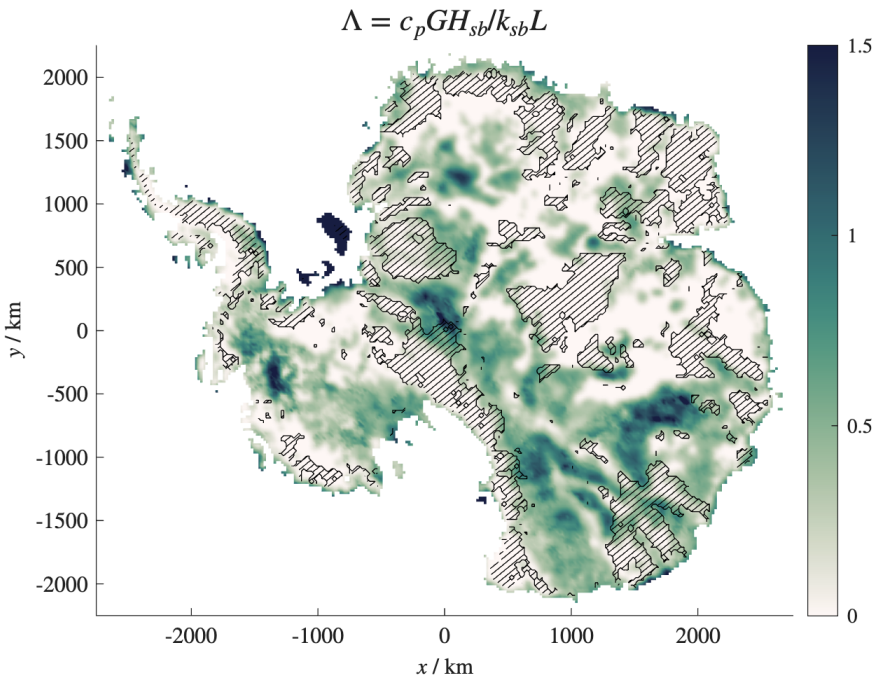

Fig. 12. Parameter $\Lambda = c_p G H_{sb}/k_{sb} L$, which roughly determines the size of the melt rate modification relative to the exfiltration.